The GOES-R Advanced Baseline Imager: Detector Spectral Response Effects on Thermal Emissive Band Calibration

Aaron J. Pearlman[a], Francis Padula[b],Changyong Cao[c], and Xiangqian Wu[c]

[a] Earth Resources Technology, Inc., Laurel, MD;
[b] GeoThinkTank, LLC, Alexandria, VA;
[c] NOAA/NESDIS/STAR, College Park, MD

1. ABSTRACT

The Advanced Baseline Imager (ABI) will be aboard the National Oceanic and Atmospheric Administration's Geostationary Operational Environmental Satellite R-Series (GOES-R) to supply data needed for operational weather forecasts and long-term climate variability studies, which depend on high quality data. Unlike the heritage operational GOES systems that have two or four detectors per band, ABI has hundreds of detectors per channel requiring calibration coefficients for each one. This increase in number of detectors poses new challenges for next generation sensors as each detector has a unique spectral response function (SRF) even though only one averaged SRF per band is used operationally to calibrate each detector. This simplified processing increases computational efficiency. Using measured system-level SRF data from pre-launch testing, we have the opportunity to characterize the calibration impact using measured SRFs —both per detector and as an average of detector-level SRFs similar to the operational version. We calculated the spectral response impacts for the thermal emissive bands (TEB) theoretically, by simulating the ABI response viewing an ideal blackbody and practically, with the measured ABI response to an external reference blackbody from the pre-launch TEB calibration test. The impacts from the practical case match the theoretical results using an ideal blackbody. The observed brightness temperature trends show structure across the array with magnitudes as large as 0.1 K for band 12 (9.61 μm), and 0.25 K for band 14 (11.2 μm) for a 300 K blackbody. The trends in the raw ABI signal viewing the blackbody support the spectral response measurements results, since they show similar trends in bands 12 (9.61 μm), and 14 (11.2 μm), meaning that the spectral effects dominate the response differences between detectors for these bands. We further validated these effects using the radiometric bias calculated between calibrations using the external blackbody and another blackbody, the ABI on-board calibrator. Using the detector-level SRFs reduces the structure across the arrays but leaves some residual bias. Further understanding of this bias could lead to refinements of the blackbody thermal model. This work shows the calibration impacts of using an average SRF across many detectors instead of accounting for each detector SRF independently in the TEB calibration. Note that these impacts neglect effects from the spectral sampling of Earth scene radiances that include atmospheric effects, which may further contribute to artifacts post-launch and cannot be mitigated by processing with detector-level SRFs. This study enhances the ability to diagnose anomalies on-orbit and reduce calibration uncertainty for improved system performance.

2. INTRODUCTION

The new generation of NOAA's environmental geostationary satellite imagers, the Geostationary Operational Environmental Satellite R-Series (GOES-R) Advanced Baseline Imager (ABI), planned to launch in 2016, will have improved spatial and temporal resolution, which require detector arrays with hundreds of detectors in each of its sixteen spectral bands.[6] The detector arrays for the TEB consist of six columns where one detector per row is used. This contrasts with current and heritage GOES imagers that only have a few detectors per channel.[7] In retrieving the effective spectral radiance or brightness temperature for ABI operations, one spectral response function (SRF) will represent each band instead of accounting for the spectral response of each detector individually. The baseline operational SRFs were derived by propagating the spectral reflectances/transmittances of the optical components and detector quantum efficiencies in the ABI optical train to obtain the SRF for each band. This process yields an SRF that is effectively a band-averaged SRF from all detectors instead of a unique spectral response based on each one. Although this strategy has demonstrated compliance to ABI's radiometric and spectral requirements, we have the opportunity to conduct research to investigate smaller effects found

Sensors, Systems, and Next-Generation Satellites XIX, edited by Roland Meynart, Steven P. Neeck, Haruhisa Shimoda, Toshiyoshi Kimura, Proc. of SPIE Vol. 9639, 963917 · © 2015 SPIE
CCC code: 0277-786X/15/$18 · doi: 10.1117/12.2195195

during pre-launch system-level SRF testing to better understand the instrument's behavior. A previous study on an advanced imager currently in operations, the Suomi National Polar-orbiting Partnership (S-NPP) Visible Infrared Imaging Radiometer Suite (VIIRS),[1] explored two types of artifacts in Earth imagery that can occur when multi-detector bands are represented by a band-averaged SRF: computational —related to the calibration process—and atmospheric —related to each detector's spectral sampling of a scene.[3] These phenomena support artifacts observed in sea surface temperature imagery, which rely on bands M15 and M16. Since we will have the same product for ABI and use analogous bands, band 14 (11.2 μm) and band 15 (12.3 μm), and expect similar noise performance, we may observe similar artifacts. In this investigation, we focus our study on the potential computational artifacts of these and other thermal emissive bands (TEB) using pre-launch test data from the system-level spectral response test and the TEB calibration test. The detector-level SRFs are investigated in the framework of the TEB calibration test to understand these artifacts. The atmospheric artifacts have been studied separately.[4]

3. SPECTRAL RESPONSE TEST AND RESULTS

The system-level spectral response test measured the SRFs for all the TEB using lamp sources that illuminated a monochromator and detected by the ABI. The monochromator swept over a range of wavelengths for each band and all the detectors within each band, so that a unique SRF was generated for each detector within each channel. This test was conducted in ambient conditions making the quality of some of the bands significantly degraded (bands 8 (6.18 μm) , 9 (6.95 μm), 10 (7.34 μm), 11 (8.50 μm)) due to water vapor absorption effects (Fig. 1). We analyzed the remaining bands (7 (3.90 μm), 12 (9.61 μm), 13 (10.35 μm), 14 (11.2 μm), 15 (12.3 μm), 16 (13.3 μm)) by determining the calibration impact of using a band-averaged SRF (averaging all detector SRFs within the band) versus the detector-level SRFs. Note that these band-averaged SRFs show differences with the operational versions, which, as mentioned, were derived using a different method. The uncertainties of the SRFs derived with the different methods are outside the scope of this work, but have been discussed for other sensors.[2] The system-level measurement results show that the detector-level SRFs in some bands seem to have less variation than others (bands 7 (3.90 μm) versus band 14 (11.2 μm), for instance). Band 14 has a systematic increase in the shoulder in high wavelength side with increasing detector number (Fig. 1).

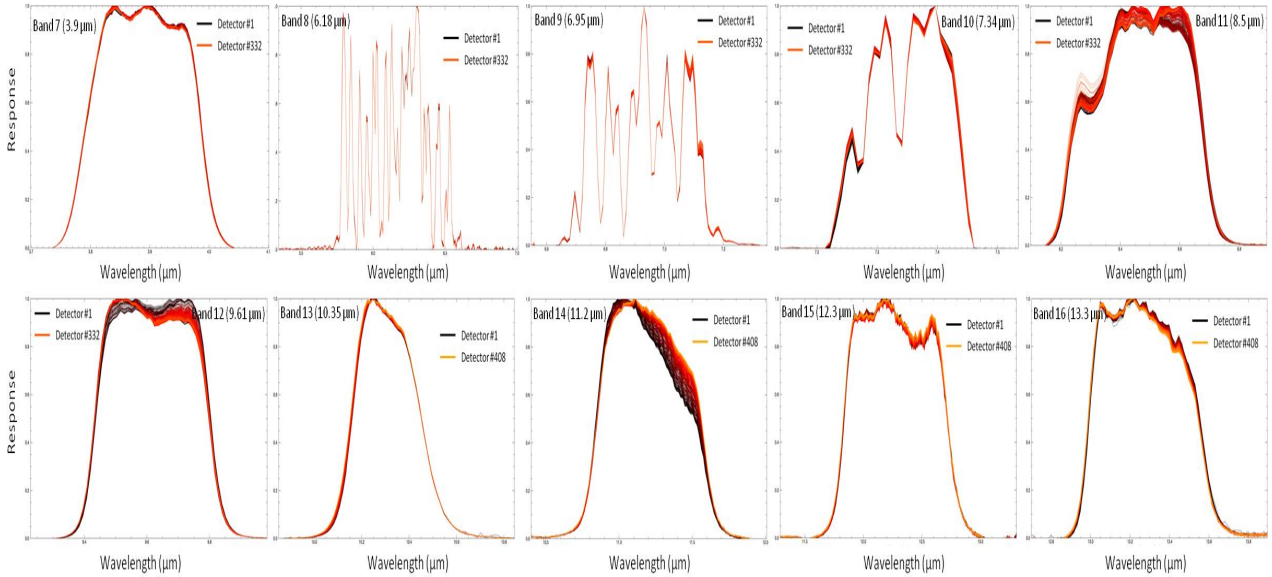

Figure 1: Detector-level spectral response functions (SRFs) for thermal emissive bands (TEB).

4. IDEAL BLACKBODY - COMPUTATIONAL ARTIFACTS

We predict the computational artifacts for an ideal blackbody of temperature (T) using Planck's Law: first, to generate the effective spectral radiance using the detector-level SRFs, and then using its inverse to retrieve the brightness temperature for each detector using the band averaged SRF for each detector. The brightness temperature assigned is subtracted by the retrieved brightness temperature for each detector to calculate the impact. Alternatively, this impact is expressed in radiance by using Planck's Law to generate the effective spectral radiances using the detector-level SRFs and the band-average SRF and calculating their difference. Figure 2 shows the radiance difference over a range of blackbody temperature values. Bands 12 and 14 have the largest trends across the arrays, equivalent to ≈0.10 K and ≈0.25 K, respectively for the 300 K blackbody case. Band 12 ($9.61\mu m$) shows a concave down feature over the first hundred detectors and band 14 ($11.2\mu m$) shows a more gradual variation across the array (≈0.25 K).

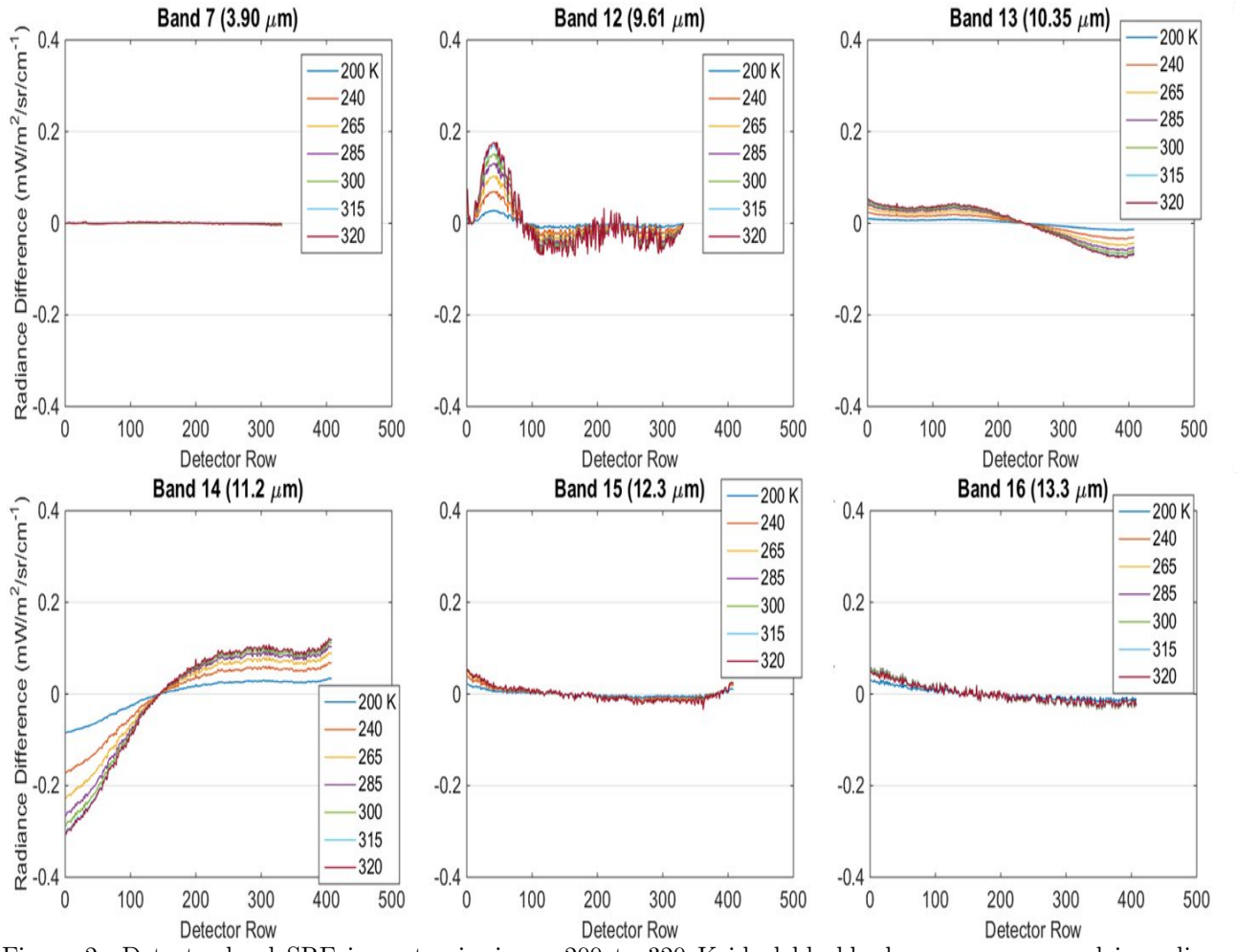

Figure 2: Detector-level SRF impacts viewing a 200 to 320 K ideal blackbody source expressed in radiance difference as a function of detector row number. Each plot shows a different channel.

5. EMISSIVE CALIBRATION TEST - COMPUTATIONAL ARTIFACTS

In order to check if these predicted effects using an ideal blackbody are realistic, we investigate them in the context of the TEB calibration test. This test was performed in a thermal vacuum chamber: Either an external blackbody, the ABI's internal (on-board) calibration blackbody, or a cold blackbody (simulating a view of deep space) illuminates the ABI as it records the signal in counts. The cold blackbody counts are subtracted from

either the internal or external blackbody to retrieve the "delta counts" (Δc) to account for the instrument offset. The calibration is done using the relationship between Δc and the effective spectral radiance (L) given by the blackbody temperature sensors and converted to radiance (L_{bb}) using Plack's Law and the SRFs (Φ):

$$L = \frac{\int L_{bb}\Phi(k)dk}{\int \Phi(k)dk}, \tag{1}$$

The calculation is done with respect to wavenumber (k), and Φ are either the band-averaged SRFs or the detector-level SRFs. The external blackbody temperature is varied from 200 K to 320 K while the internal blackbody is held fixed at 295 K (used for this study) or 309 K. The calibration accounts for the differences in the optical paths between different view positions. This is captured in terms that represent the emissivity/reflectance of ABI's two scan mirrors: the north-south (NS) and east-west (EW). When they view different positions, their reflectances and emissivities, ρ and ε, differ due to their angular dependence. The calibration equation for a blackbody (denoted bb) is derived by first expressing the radiance contributions from the blackbody and the NS and EW scan mirrors (in terms of ρ and ε, respectively) viewing the blackbody and another cold blackbody (sp) (to represent an on-orbit space look) and equating them each with a polynomial expression in terms of ABI counts (c) with linear (m) and quadratic (q) coefficients. The mirror reflectance values' angular dependence are denoted by the superscript —for instance, ρ_{NS}^{bb} means the reflectance of the NS mirror at the blackbody view position:

$$L^{bb}\,\rho_{NS}^{bb}\,\rho_{EW}^{bb} + \varepsilon_{NS}^{bb}\,L_{NS}\,\rho_{EW}^{bb} + \varepsilon_{EW}^{bb}\,L_{EW} = qc_{bb}^2 + mc_{bb} \tag{2a}$$

$$L^{sp}\,\rho_{NS}^{sp}\,\rho_{EW}^{sp} + \varepsilon_{NS}^{sp}\,L_{NS}\,\rho_{EW}^{sp} + \varepsilon_{EW}^{sp}\,L_{EW} = qc_{sp}^2 + mc_{sp} \tag{2b}$$

Subtracting Eq. 2b from 2a and using $\Delta c = c_{bb} - c_{sp}$ yields the calibration equation:

$$\Delta L = L^{bb}\,\rho_{NS}^{bb}\,\rho_{EW}^{bb} - L^{sp}\,\rho_{NS}^{sp}\rho_{EW}^{sp} + L_{offset} = q\Delta c_{bb}^2 + m\Delta c_{bb}, \texttt{ where} \tag{3a}$$

$$L_{offset} = L_{NS}\,(\varepsilon_{NS}^{bb}\,\rho_{EW}^{bb} - \varepsilon_{NS}^{sp}\,\rho_{EW}^{sp}) + L_{EW}\,(\varepsilon_{EW}^{bb} - \varepsilon_{EW}^{sp}) \tag{3b}$$

The blackbody emissivities are neglected in the equations as they are assumed unity. The SRFs are used in calculating L and in converting between brightness temperature and L. Comparing ABI's calibration using the external blackbody to its calibration using the internal blackbody can be used to validate the on-board calibration. We will compare them using either band-averaged SRFs or the detector-level SRFs. But first, we use only the external blackbody to see how well the ABI's behavior in a real measurement environment matches the prediction from an ideal blackbody case with respect to SRF effects. Pre-launch measurements have shown that the linearity of all TEB are high and the q terms are negligible. Given this, we expect that if we introduce detector-level calibration, the trends found for the ideal blackbody case will be maintained in the test environment. Figure 3 shows that the expected trend in radiance difference —L^{bb} calculated with detector-level SRFs minus L^{bb} calculated using an averaged SRF—is maintained but with a channel-dependent offset. This offset is related to the fitting residuals from the calibration equation. (It is also likely a manifestation of the limitations of the blackbody thermal model used to calculate the effective brightness temperature.[5])

Since the previous analysis assumed the existence of detector-level SRFs, we want to see if the raw instrument counts themselves reveal the effects predicted by the spectral response results; if the detector differences are dominated these effects, they should be reflected in the raw ABI signals across the arrays. For instance, in the extreme case, if we assume that the gains of all detectors are identical and non-linearity is negligible, and all differences between detectors can be attributed to SRF differences, the Δc would be proportional to the effective spectral radiance calculated with detector-level SRFs over the array. In our case, the spectral radiances and Δc are not strictly proportionality but their trends match closely in bands 12 ($9.61\mu m$) and 14 ($11.2\mu m$) (Fig. 4). Note that bands 13-16 are inverted, making the Δc values negative, so the absolute value of the Δc should be taken before comparing to the spectral trends (in Fig. 4). The raw signals suggests that these measured detector-level spectral effects are real and dominate the response difference between detectors for these channels.

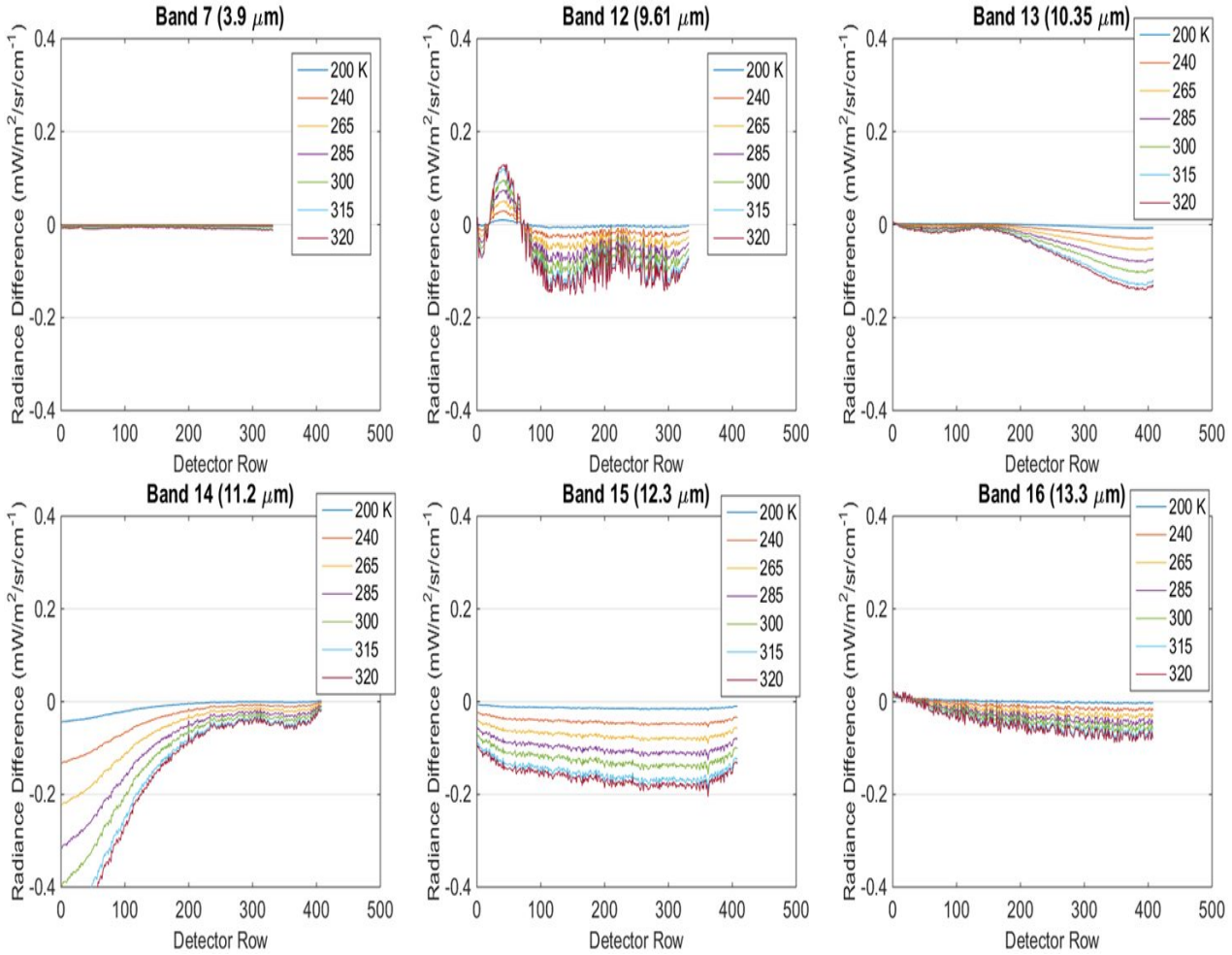

Figure 3: Detector-level SRF impacts expressed in radiance difference as a function of detector row number. These are calculated by propagating the measured detector-level SRFs and band-averaged SRFs through the emissive channel calibration for the external blackbody set to 200 to 320 K. Each plot shows a different channel.

6. EMISSIVE CALIBRATION TEST - CALIBRATION BIAS

To further analyze the impacts of using detector-level SRFs versus band-averaged SRFs, we compare the calibrations using the internal (int) and external (ext) blackbody by applying the m coefficient derived from the internal blackbody view and applying it to the ABI response to the external blackbody. The radiance/brightness temperature is compared to that given by the blackbody temperature:

$$m_{int} = \frac{L^{int}\,\rho^{int}_{NS}\,\rho^{int}_{EW} + L^{int}_{offset}}{\Delta c_{int}} \tag{4a}$$

$$L_{ext} = \frac{m_{int}\Delta c_{ext} - L^{ext}_{offset}}{\rho^{ext}_{NS}\,\rho^{ext}_{EW}} \tag{4b}$$

The radiance from the cold blackbody and the quadratic term in the polynomial are neglected. We convert L_{ext} to brightness temperature using Planck's Law and subtract the temperature of the external blackbody to obtain the radiometric bias. We calculate these temperature differences using detector-level SRFs and band-averaged SRFs for bands 12 ($9.61\mu m$) and 14 ($11.2\mu m$), since they show the largest detector-level SRF impacts. The trend

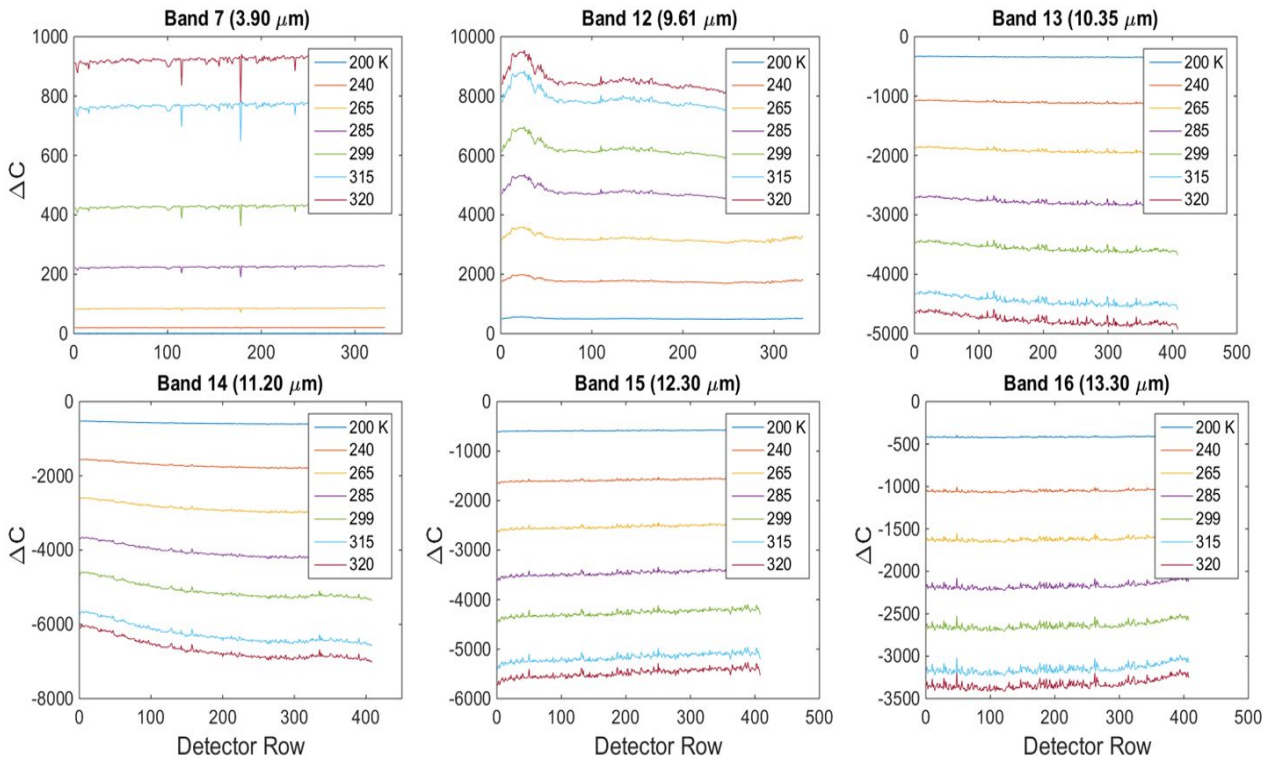

Figure 4: The trend in the ABI signal in Δc across the arrays while viewing the external blackbody varied through a range of temperature. A trend matching the detector-level SRF impacts shows that this effect dominates the differences in detector response.

flattens across the array when detector-level SRFs are used but some residual bias remains (Fig. 5). This bias is likely dominated by the limitations in the external blackbody thermal model, so the on-orbit calibration bias is expected to be lower.[5] The flattened trends using the detector-level SRFs show that the differences across the array may be mitigated.

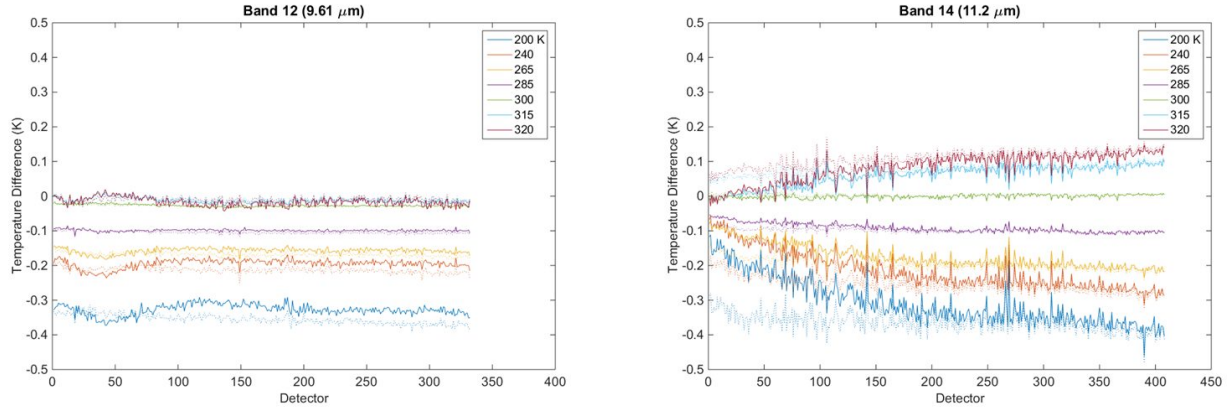

(a) (b)

Figure 5: Calibration bias between internal an external blackbody using detector-level SRFs (dotted) and band-averaged SRFs (solid).

7. CONCLUSION

We investigated the spectral effects of ABI TEB using pre-launch test data and showed the computational impacts of using a band-averaged SRFs, as planned for operations, instead of accounting for each individual detector's SRF. Simulation results from the system-level SRF measurement show the largest impacts in bands 12 ($9.61\mu m$) and 14 ($11.2\mu m$). The TEB calibration test results showed these impacts in the raw instrument response as these spectral effects dominated the differences between detectors in these channels. The application of the calibration equation maintained these impacts, and the radiometric bias calculated between calibrations using the internal and external blackbody showed that using the detector-level SRFs reduced the trends across the detector arrays. The combination of the raw count response and radiometric bias show that the spectral response test produced results that reflect the real behavior of the instrument —the test has the fidelity to reveal detector-specific behavior. Although ABI is expected to meet its radiometric requirements, these detector-level SRFs could be used to reprocess on-orbit data to reduce calibration uncertainties. This processing will be ineffective, however, in removing striping caused by atmospheric artifacts, since each detector will sense a different effective spectral radiance. This study shows how instrument performance can present across pre-launch instrument tests. It also may aid in understanding on-orbit striping artifacts especially in conjunction with studies using radiative transfer simulations.

8. ACKNOWLEDGMENTS

This work is supported by the GOES-R Program. The manuscript contents are solely the opinions of the authors and do not constitute a statement of policy, decision, or position on behalf of NOAA or the U.S. government.

REFERENCES

1. C. Cao, F.J. De Luccia, Xiaoxiong X., R. Wolfe, and F. Weng. Early on-orbit performance of the Visible Infrared Imaging Radiometer Suite onboard the Suomi National Polar-Orbiting Partnership (S-NPP) satellite. *Geosc. and Remote Sensing, IEEE Trans. on*, 52(2):1142–1156, Feb 2014.
2. S. Hansen, J. Peterson, R. Esplin, and J. Tansock. Component level prediction versus system level measurement of SABER relative spectral response. *Int J Remote Sens*, 24(2):389–402, 2003.
3. F. Padula and C. Cao. Detector-level spectral characterization of the Suomi National Polar-orbiting Partnership Visible Infrared Imaging Radiometer Suite long-wave infrared bands M15 and M16. *Appl. Opt.*, 54(16):5109–5116, Jun 2015.
4. F. Padula and C. Cao. GOES-R ABI detector-level spectral response function performance characterization. IGARSS Proceedings, 2015.
5. A. Pearlman, R. Datla, C. Cao, and X. Wu. Multichannel IR sensor calibration validation using Planck's Law for next generation environmental geostationary systems. In *Calcon Technical Meeting: Meeting on Characterization and Radiometric Calibration for Remote Sensing*, 2015.
6. T. Schmit, M. Gunshor, W.P. Menzel, J. Gurka, J. Li, and A. Bachmeier. Introducing the next-generation Advanced Baseline Imager on GOES-R. *Bull. Amer. Meteor. Soc.*, 86(5):1079–1096, 2005.
7. E. Wack, M. Weinreb, and J. Lawrence. Prelaunch infrared calibration of the GOES I-M imager and sounder. *Proc. SPIE*, 4135:140–149, 2000.